Environmental Pollution 276 (2021) 116707

Contents lists available at ScienceDirect

Environmental Pollution

journal homepage: www.elsevier.com/locate/envpol

New global aerosol fine-mode fraction data over land derived from MODIS satellite retrievals☆

Xing Yan [a], Zhou Zang [a], Chen Liang [a], Nana Luo [b], Rongmin Ren [a], Maureen Cribb [c], Zhanqing Li [c, *]

[a] State Key Laboratory of Remote Sensing Science, College of Global Change and Earth System Science, Beijing Normal University, Beijing, 100875, China
[b] Department of Geography, San Diego State University, 5500 Campanile Dr., San Diego, CA, 92182-4493, USA
[c] Department of Atmospheric and Oceanic Science and ESSIC, University of Maryland, College Park, MD, 20740, USA

ARTICLE INFO

Article history:
Received 13 November 2020
Received in revised form
15 January 2021
Accepted 5 February 2021
Available online 8 February 2021

Keywords:
Fine-mode fraction
Global scale
MODIS
Trend

ABSTRACT

The space-borne measured fine-mode aerosol optical depth (fAOD) is a gross index of column-integrated anthropogenic particulate pollutants, especially over the populated land. The fAOD is the product of the AOD and the fine-mode fraction (FMF). While there exist numerous global AOD products derived from many different satellite sensors, there have been much fewer, if any, global FMF products with a quality good enough to understand their spatiotemporal variations. This is key to understanding the global distribution and spatiotemporal variations of air pollutants, as well as their impacts on global environmental and climate changes. Modifying our newly developed retrieval algorithm to the latest global-scale Moderate Resolution Imaging Spectroradiometer (MODIS) aerosol product (Collection 6.1), a global 10-year FMF product is generated and analyzed here. We first validate the product through comparisons with the FMF derived from Aerosol Robotic Network (AERONET) measurements. Among our 169,313 samples, the satellite-derived FMFs agreed with the AERONET spectral deconvolution algorithm (SDA)-retrieved FMFs with a root-mean-square error (RMSE) of 0.22. Analyzed using this new product are the global patterns and interannual and seasonal variations of the FMF over land. In general, the FMF is large (>0.80) over Mexico, Myanmar, Laos, southern China, and Africa and less than 0.5 in the Sahelian and Sudanian zones of northern Africa. Seasonally, higher FMF values occur in summer and autumn. The linear trend in the satellite-derived and AERONET FMFs for different countries was explored. The upward trend in the FMFs was particularly strong over Australia since 2008. This study provides a new global view of changes in FMFs using a new satellite product that could help improve our understanding of air pollution around the world.

1. Introduction

Atmospheric aerosols, particularly anthropogenic aerosols, have major influences on the environment (Zheng et al., 2015; Komkoua et al., 2017; C. Li et al., 2017; Luo et al., 2015; Luo et al., 2016; Yang et al., 2018), clouds and precipitation (J. Li et al., 2019; Y. Liu et al., 2019; Singh et al., 2019), and Earth's climate in general (Allen et al., 2016; IPCC, 2013; Nakata et al., 2017). Even though the significance of anthropogenic aerosols has been widely recognized, fine-mode aerosol datasets with a quality good enough for analyzing and understanding their spatiotemporal variations on a global scale are scarce. Kaufman et al. (2002) pioneered the inference of aerosol size on a global scale, noting a gross connection between the fine-mode aerosol loading and population and anthropogenic activities. Given aerosol optical depth (AOD) retrievals at multiple channels, satellite sensors can detect the fine-mode fraction (FMF, defined as the fraction of the fine-mode aerosol amount to the total aerosol amount) then calculate the fine-mode AOD (fAOD, fAOD = FMF × AOD). Atmospheric particles characterized by the fAOD usually have submicron diameter sizes and are mostly anthropogenic (Chung et al., 2016; Jethva et al., 2007; Levy et al., 2013; Yan et al., 2017a). Good knowledge of the FMF on a global scale is thus key to understanding the impacts of anthropogenic aerosols on global climate change and the environment.

☆ This paper has been recommended for acceptance by Pavlos Kassomenos.
* Corresponding author.
E-mail address: zli@atmos.umd.edu (Z. Li).

https://doi.org/10.1016/j.envpol.2021.116707
0269-7491/

Major contributors to atmospheric extinction in many locations are fine-mode particles (Adak et al., 2014; Che et al., 2014). Many studies have confirmed the importance of the FMF in exploring the anthropogenic aerosol radiative effect (Bellouin et al., 2005; Chung et al., 2016) and in estimating particulate matter with diameters less than 2.5 μm ($PM_{2.5}$; Zhang and Li, 2015). However, it is still a challenge to obtain reliable spatial coverage maps of the FMF, especially on a global scale (Yan et al., 2018; Yang et al., 2020). The Moderate Resolution Imaging Spectroradiometer (MODIS), the first satellite sensor to provide sound-quality retrievals of AOD over land, generates global AOD products on a daily basis at different wavelengths (Remer et al., 2005). MODIS aerosol products have been continually updated since 2000, culminating in the latest product, Collection 6.1 (C6.1). Currently, there are two aerosol algorithms providing FMF data in MODIS C6.1: the Dark Target (DT) algorithm and the Multi-Angle Implementation of Atmospheric Correction (MAIAC) algorithm (Lyapustin et al., 2018). However, the MAIAC currently offers FMFs over the oceans only. Although the MODIS DT aerosol product is continually updated, the FMF is still highly uncertain over land (Levy et al., 2013). Levy et al. (2007) indicated that compared to the Aerosol Robotic Network (AERONET) FMF, the MODIS FMF has improved from C4 to C5, with the coefficient of determination (R^2) increasing from 0.067 to 0.248. However, Jethva et al. (2007) showed that the accuracy of the FMF in C5 was less than that of C4, with the correlation with AERONET FMFs decreasing from 0.74 to 0.43. Redemann et al. (2009) also found a deterioration in R^2 from C4 to C5, going from 0.177 to 0.02 (Terra) and from 0.232 to 0.126 (Aqua). As discussed by Levy et al. (2013), MODIS-based FMF data over land are still experimental and highly uncertain but still provided in the C6 series of along-orbit (Level 2) aerosol products (MOD04 and MYD04). The paucity of global FMF data over land hinders our ability to study anthropogenic aerosols on a global scale. However, the FMF may be determined from ground-based measurements. Ground-based aerosol observation networks include the AERONET (Holben et al., 1998), the SKYrad Network (Takamura and Nakajima, 2004), the China Aerosol Remote Sensing Network (Che et al., 2009), and the Sun-sky radiometer Observation NETwork (Z. Q. Li et al., 2018), among others. O'Neill et al. (2001) developed a spectral deconvolution algorithm (SDA) to derive the FMF using AERONET spectral solar extinction data, validated with in situ airborne measurements by Gassó and O'Neill (2006). The SDA emphasized that fine and coarse mode optical depths are defined optically and that the FMF derived represents fine AOD at a particular wavelength/total AOD (O'Neill et al., 2003). Kleidman et al. (2005) indicated that compared with the Dubovik inversion method (Dubovik et al., 2000), an SDA is more appropriate for exploring anthropogenic versus naturally occurring atmospheric aerosols. Although AERONET-based SDA FMF measurements are accurate, each represents only a small area. By contrast, satellites offer global coverage, but the estimated FMF is much less accurate (Kleidman et al., 2005). Applying the same principles laid out by O'Neill et al. (2001), Yan et al. (2017b) developed a look-up table spectral deconvolution algorithm (LUT-SDA) to improve the FMF retrieval on a city scale. Yan et al. (2019) further enhanced this algorithm by accounting for the seasonal characteristics of aerosol properties for regional-scale FMF retrievals in Asia.

This study first modifies the algorithm developed by Yan et al. (2017b, 2019) then employs it to generate a new global long-term (2008–2017) FMF dataset for land. Based on this new dataset, examined are the spatial and temporal variations in FMF over land around the world. Causes for the interannual variability, long-term trends, and regional differences are explored. A comprehensive discussion of the differences between this product and the MODIS FMF product is also presented.

2. Materials and methods

2.1. Satellite data

A complete 10-year (2008–2017) MODIS (Terra) Level-3 Collection 6.1 daily global aerosol AOD products (MOD08 DT-based) database was obtained (https://ladsweb.nascom.nasa.gov) for this study. The spatial resolution is 1 ° × 1 °, and the L2 MODIS aerosol product forms the basis of each grid cell value. The main features of MOD08 are the data quality checks and the reduction in random noise (Ruiz-Arias et al., 2013). However, there are some inconsistencies between MODIS Terra and Aqua data, especially for AOD (Sayer et al., 2015; Levy et al., 2018). In our previous studies, the MODIS (Terra) aerosol products had been applied for FMF retrieval at the urban (Yan et al., 2017b) and regional scales (Yan et al., 2019). Thus, in this study, we continued to use these products (Yan et al., 2019) to estimate FMF at the global scale. For global FMF retrieval, historical AERONET data are needed for LUT-SDA to create LUT. The variable *Aerosol_Optical_Depth_Land* from the MOD08 product provides AODs at the blue (0.47 μm) and red (0.66 μm) bands (Quality Assurance $\geq$ 2); these are used to calculate the Ångström exponent (AE) and AOD at 500 nm. Given the removal of the C6.1 MOD08 FMF product from the NASA archive (Levy et al., 2013), an earlier version of the FMF from C5 (Levy et al., 2007), available from the NASA Earth Observations website (https://neo.sci.gsfc.nasa.gov/), is used for comparison.

2.2. AERONET

Owing to the limitations in Version 3 AERONET data at the time when we conducted this study, we used Version 2 (Smirnov et al., 2000) Spectral Deconvolution Algorithm (SDA) products (Level 2 data) for 176 AERONET sites (Fig. 1a) (Holben et al., 1998). The SDA inversion products, which are based on AERONET-measured AOTs at different wavelengths (with an uncertainty of ~0.01 in visible and near IR bands; Eck et al., 1999), can provide FMF and AE derivative (α') data. The latter describes the deviation from linearity of the AOT variation in logarithmic coordinates, which was first introduced and defined by Eck et al. (1999). The α' conveys aerosol size information: large positive values are attributed to a high fraction of fine-mode aerosols, and near-zero and negative values denote high fractions of coarse-mode aerosols (O'Neill et al., 2001). Based on Yan et al. (2019), α' obtained from the last five years of AERONET data was used to determine the seasonal α' and retrieve the next year's global FMF. For example, the AERONET data for 2003–2007 was used to examine the general range of α' for LUT-SDA to retrieve the 2008 global FMF.

2.3. Global FMF retrieval

This study uses a LUT-SDA for retrieving FMFs over land on a global scale (Yan et al., 2017b). This method follows the SDA first proposed by O'Neill et al. (2001) and is modified here for global satellite-based FMF retrieval. A set of hypothetical values for α' (determined by historical AERONET data from different locations), the AE (0–2.5), and the AE of fine-mode AOD (0–2.5) and AOD (0–5) are imported to the SDA to calculate the FMF and to create the LUT. For the global-scale LUT-SDA, we first clustered the study domain into nine regions (Fig. 1b) based on Sayer et al. (2014). Historical AERONET measurements were then used to determine the α' range of values in the different regions based on the first and third quartiles of the data in each season (Yan et al., 2019). This showed that accounting for seasonal changes instead of using an annual range for α' improves the FMF retrieval accuracy in Asia; therefore, we tested this method further for global application (Yan

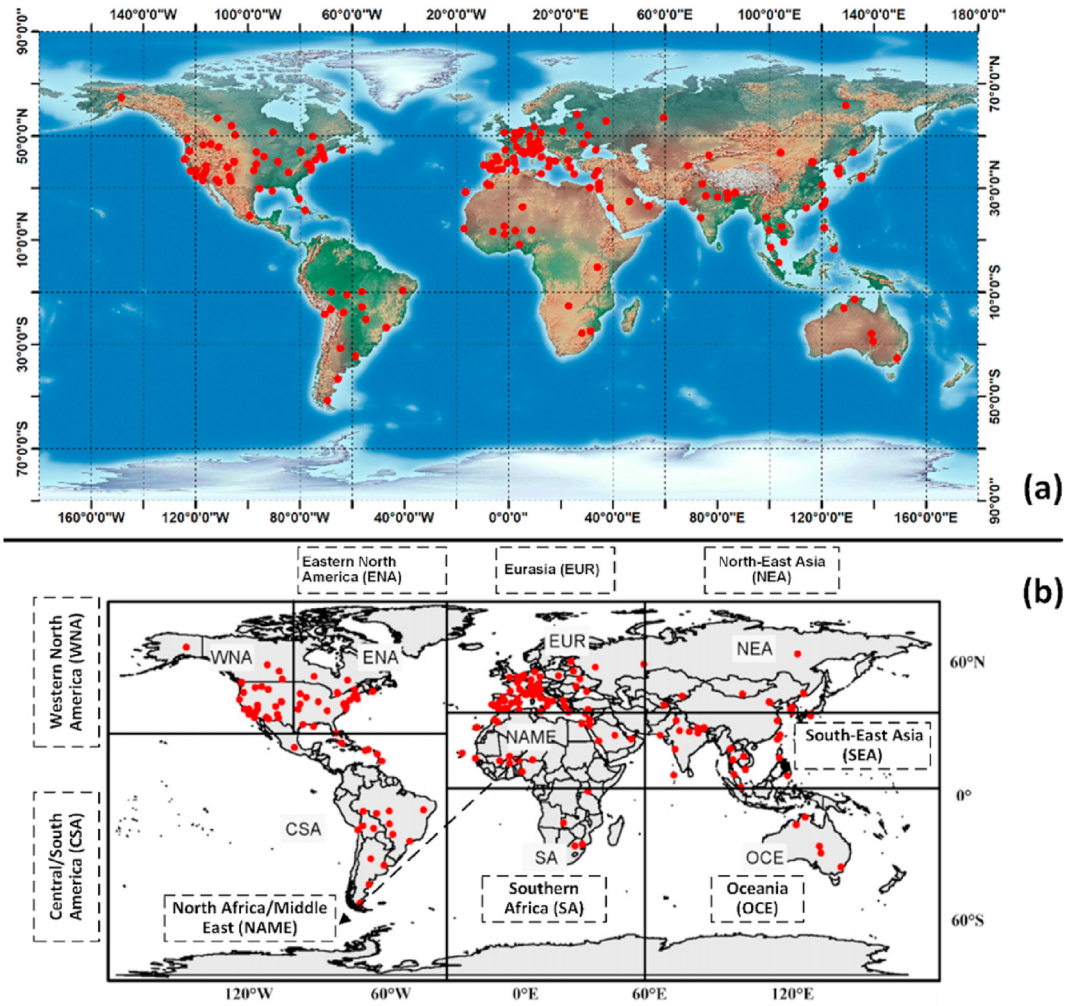

Fig. 1. (a) Locations of AERONET stations used in this study. (b) The clustered nine regions in this study for LUT-SDA FMF retrieval. The names of the regions and their abbreviations are: Eastern North America (ENA), Western North America (WNA), Central/South America (CSA), Eurasia (EUR), North Africa/Middle East (NAME), Southern Africa (SA), North-East Asia (NEA), South-East Asia (SEA), and Oceania (OCE).

et al., 2019). Figure S1 presents the histograms of α' from 2008 to 2017 for nine regions. The figure shows great spatial heterogeneity among these regions. According to O'Neill et al. (2001) and Eck et al. (2010), a large α' indicates the dominance of fine-mode aerosols, while α' close to or less than 0 is characteristic of coarse-mode aerosols. It is evident that ENA, EUR, SA, NEA, and SEA are fine-mode aerosol-dominated regions ($\alpha' > 0$) where the FMF is also high (>0.72). The largest α' occurs over SEA, corresponding well with the very high FMF there (>0.8). The LUT-SDA attempts to find the FMF that exactly matches the following:

$$\text{Minimum}\Big[(LUT - SDA_{AE} - \text{MODIS}_{AE})^2 + (LUT - SDA_{AOD} - \text{MODIS}_{AOD})^2\Big] \quad (1)$$

where MODIS_{AOD} is the MOD08 DT-based AOD at 500 nm, and MODIS_{AE} is the MOD08 DT-based AE. Both are calculated from 0.47 μm to 0.66 μm MOD08 DT-based AOD.

2.4. Linear trend and analysis of relative change

A linear trend has been applied in many studies to calculate the temporal variation in aerosol conditions (Hsu et al., 2012; Che et al., 2019). In this study, a simple least-squares fit was used to obtain the slope coefficient of the linear regression as the trend for FMFs, as follows:

$$Y_t = \beta_0 + \beta_1 X_t + \varepsilon \quad (2)$$

where Y_t is the monthly FMF, and X_t is the years in the time series ($X_t = t/12$, $t = 1,2,\ldots,T$, where T is total number of year). β_0 and β_1 are determined by the least-squares method, ε is the error term, the F test was used to assess the trend in the estimates, and statistical significance was determined at a 95% confidence level.

We also calculated the relative change between the first and last 5-year FMF as the percentage of changes in the FMF from 2008 to 2017 (Mehta et al., 2016):

$$\text{Relative Change} = \frac{M_{2017-2013} - M_{2012-2008}}{M_{2012-2008}} \times 100\% \quad (3)$$

where $M_{2017-2013}$ is the mean FMF value for the period 2013–2017, and $M_{2012-2008}$ is the mean FMF value for the period 2008–2013.

3. Results

3.1. Validation and comparison

The FMF retrievals from 176 worldwide AERONET sites were validated against the new global daily FMF products for the period 2008–2017 (Fig. 2a). High kernel density values (dark red areas) show where most of the data lie. The new FMF product, with its RMSE of 0.22 and R of 0.41, is consistent with ground-based observations. Fig. 2a also shows that there are two dense centers around 0.9 and 0.65. Fine-mode particles dominate the high FMF domain, while mixed-mode aerosols dominate the other domain. This mixed-mode aerosol type has been found in many areas, such as Chennai and Mumbai in India (Ramachandran, 2007) and in East Asian countries (Kim et al., 2007) such as China, Korea, and Japan, where fossil fuel emissions, biogenic aerosols, man-made aerosols, dust, and sea salt combine to make composite aerosols.

Fig. 2b plots the new FMF product against the AERONET FMF

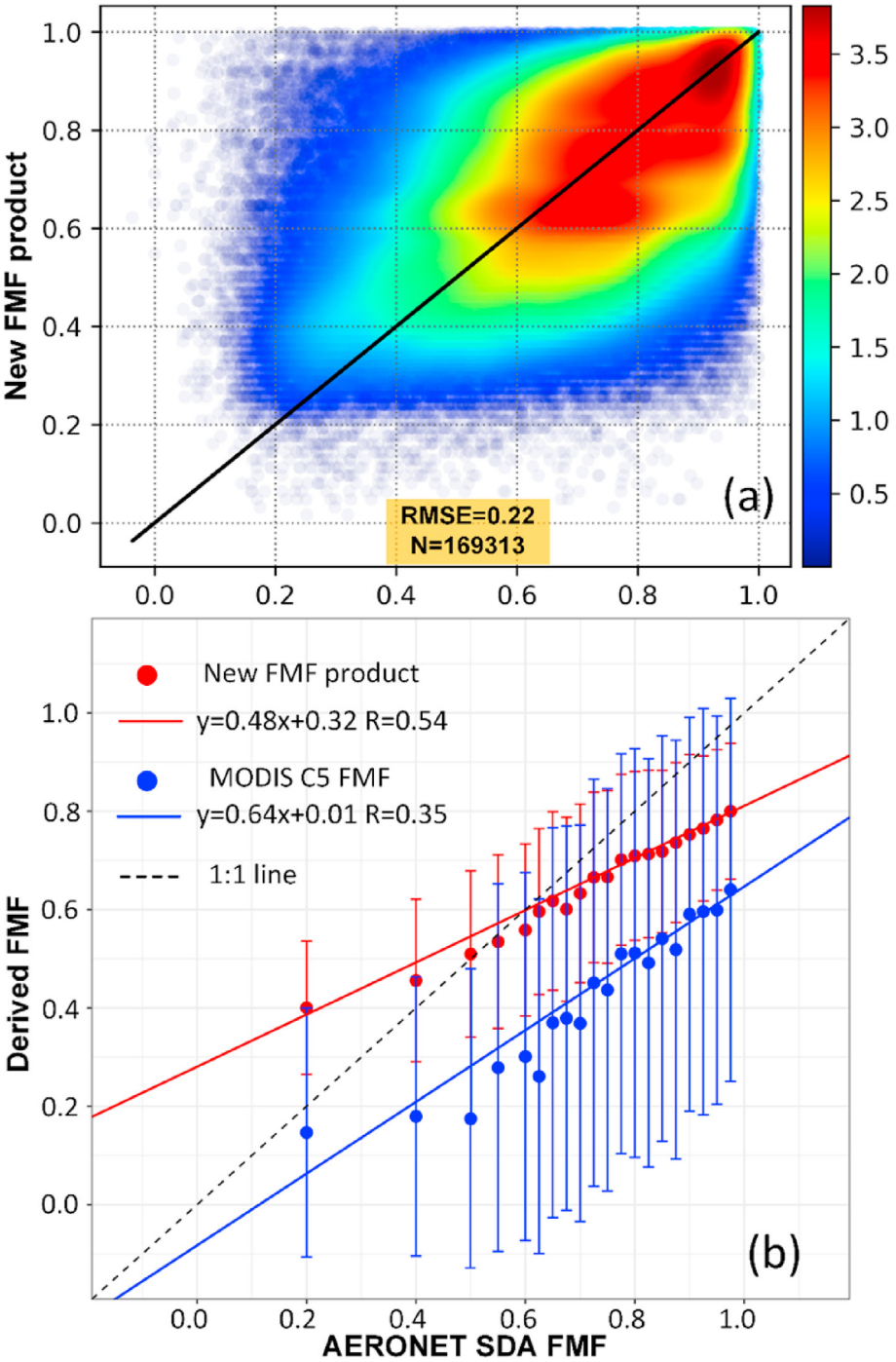

Fig. 2. (a) Comparison of LUT-SDA and AERONET-retrieved FMFs using data from all global sites. The black solid line is the 1:1 line. (b) Comparison of the new FMF product and MODIS C5 FMF with AERONET measurements (AOD > 0.2). The solid circle and error bars represent the mean and standard deviation of the retrievals in 20 bins of AERONET FMF. The red and blue solid lines are the lines of best fit from the linear regression of all derived points; the black dashed line is the 1:1 line. Note that the MODIS C5 FMF is at 550 nm and that AERONET 550 nm FMF was used for validation. (For interpretation of the references to color in this figure legend, the reader is referred to the Web version of this article.)

data. We compared the new FMF product and MODIS C5 FMF with AERONET measurements AOD >0.2 based on the method in Levy et al. (2007). The two satellite datasets were extracted over 176 AERONET stations and averaged into each bin with equal numbers of observations. Compared with the MODIS C5 FMF, the new FMF product improved the correlation with AERONET measurements markedly, going from R = 0.35 to R = 0.54 (Fig. 2a). Levy et al. (2007) indicated that the improvement in the MODIS-based FMF product is mainly because of its correlation to AERONET FMF; in their validation of global MODIS C5.2 FMF, the R^2 is 0.248. Furthermore, the averaged FMF value in each bin shows that underestimations in the MODIS C5 FMF were largely improved in the new FMF product.

Fig. 3 presents an accuracy assessment of the new FMF product over land at each AERONET site (Fig. 3a and b) as well as the AOD distribution over land from 2008 to 2017 (Fig. 3c). Good accuracy (low RMSE with values < 0.15 and high R with values > 0.3) was achieved in most sites throughout the northern United States, regions of Amazonia, Western Europe, India, East Asia, and Australia. Considering that ground FMF measurements are defined only if the AOD is over a threshold that creates a sufficiently strong signal to detect FMF (Dubovik et al., 2002) and that FMF retrievals were found not found to be optimal in regions where AOD was low, a closer examination of the accuracy of new FMF products over

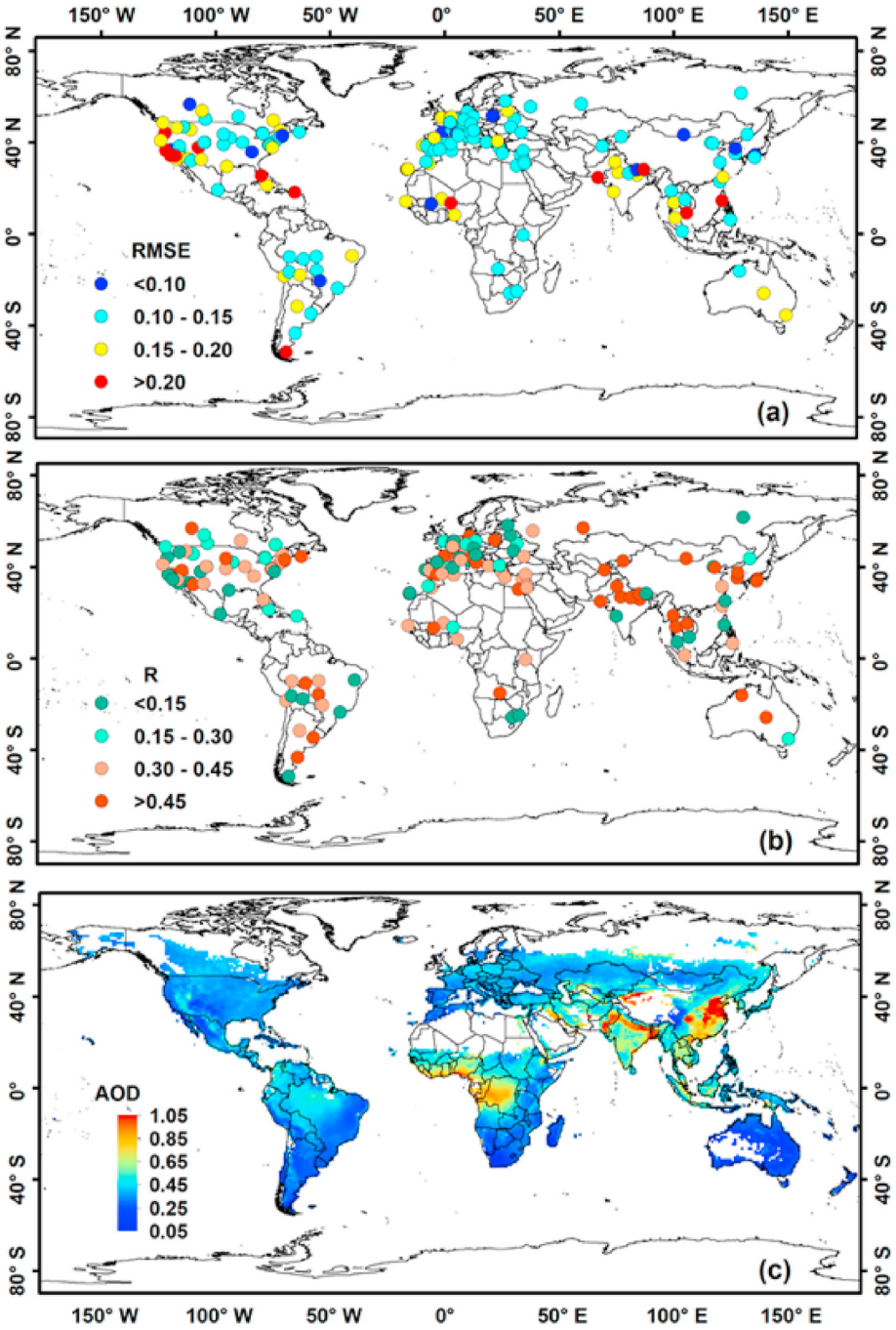

Fig. 3. Accuracy assessment of the new FMF product over land at each AERONET site from 2008 to 2017 in terms of (a) root-mean-square error (RMSE) and (b) correlation coefficient (R). (c) Shows the average MODIS DT AOD during this ten-year period (only pixels with over 120 AOD retrievals/year was considered).

regions with a high/low AOD is necessary. By comparing the RMSE and R of the new FMF product with those in regions where low and high AODs were dominant, it becomes clear that a low RMSE (<0.15) and high R (>0.3) appear over regions with a high AOD (>0.5), such as central Africa, India, and eastern China. However, areas with high RMSE (>0.15) and low R (<0.15) are concentrated mainly over regions with a low AOD (<0.2), such as the coastal regions of South America and southern Africa. Furthermore, the RMSE values of the new FMF product for some regions like Europe and Australia are moderate (<0.2), but the R values are high (>0.3) despite their low AODs.

Fig. 4 shows the 2008–2017 mean spatial distributions of the global FMF product from this study (Fig. 4a), in addition to the MODIS FMF (Fig. 4b) and the AERONET FMF products (dots). The data are from locations where there were observations for at least 120 days per year and 20 days per year with the new FMF retrievals and MODIS FMF, respectively. In comparison with the AERONET FMF, the MODIS FMF data show serious underestimation over eastern China, northern India, and the central United States, whereas the new FMF retrievals show good consistency with the AERONET FMF data. Furthermore, in regions with no MODIS FMF coverage, such as Australia and the eastern United States, the new FMF retrievals show good agreement with the AERONET FMF data. Spatially, the two products share some common gross patterns, but the new product has greater global coverage, revealing more details, and somewhat different magnitudes that vary from location to location.

From Fig. 4a, generally, FMF >0.8 appear in populated regions such as eastern North America, Mexico, central South Africa, Europe, northeastern Asia, southern Africa, and southern China. Low FMF occurs in virtually all desert or semi-desert regions, most prominently in the Sahelian and Sudanian zones of northern Africa. As noted by Eck et al. (2010), northern Africa always experiences very high loadings of desert dust from the Sahara and Sahel during most of the year. For example, in Ilorin, Nigeria (northern Africa), the mean AERONET-retrieved FMF is < 0.5 for most months (Eck et al., 2010). Seen in China is a "southern high and northern low" pattern in the FMF distribution, also reported by Tan et al. (2015).

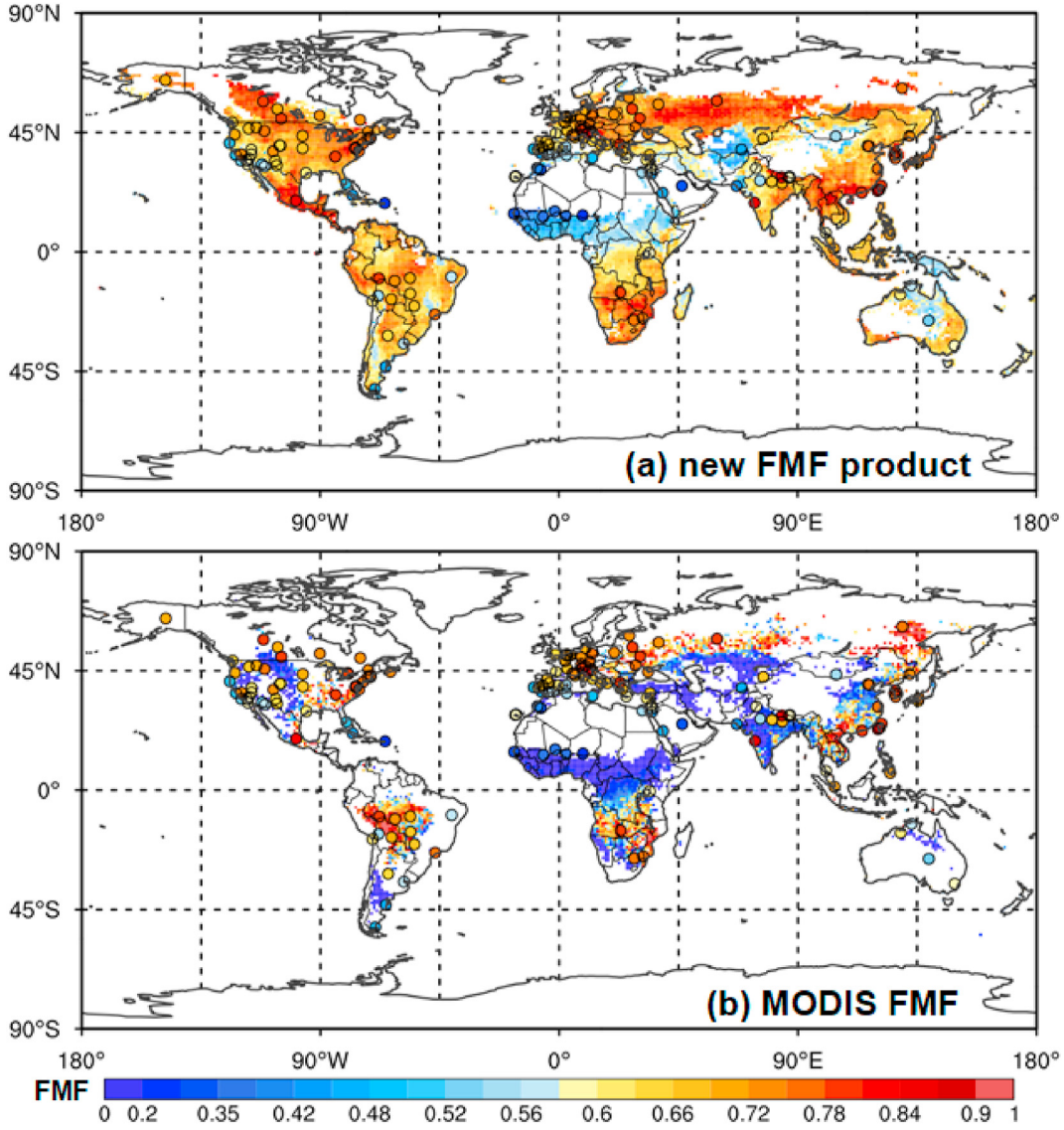

Fig. 4. Base maps depicting 2008–2017 spatial distributions of average FMF products from this study (a) and from the MODIS DT algorithm (b). The dots represent the 2008–2017 average FMF values from AERONET, using the same color bar as the base maps. (For interpretation of the references to color in this figure legend, the reader is referred to the Web version of this article.)

The low FMF over northern China where vegetation is scarce could result from dust aerosol emissions from bare land. The high FMF in southern China is associated with human activities and anthropogenic aerosol emissions, mainly fine particles (Yan et al., 2020). However, Tan et al. (2015) suggested that the high FMF in southern China is partly due to the dense vegetation that produces large amounts of biogenic compounds, mainly submicron aerosols (Carslaw et al., 2010). Seen in South Africa is an "eastern high and western low" pattern in the FMF distribution associated with burning and dust events, and human activities that are more intensive in the eastern part of the country than in the western part (Kumar et al., 2014). In the Mediterranean region, the FMFs of Eastern Europe and Turkey are higher than those in the eastern Sahara and the Middle East. Industrial and vehicular emissions from megacities in Europe, as well as wildfires in Mediterranean Europe, could result in higher FMF values (Turco et al., 2018; Tutsak et al., 2019). Mineral dust sources in the Sahara and the Middle East could directly increase local coarse emissions or transport to Mediterranean regions (Hatzianastassiou et al., 2009), leading to low FMFs. In North America, the FMF in the western U.S. is lower than that in the eastern U.S., which results from differences in landscape, population, and industrial activities. The Great Basin Desert (the largest U.S. desert), the Mojave Desert, and the Sonoran Desert are all located in the western U.S. (see Figure S2), leading to a large fraction of coarse-mode aerosol emissions in that part of the U.S. High FMF values in South America are located in the Amazon region, mainly ascribed to the frequent biomass burning occurring there (Ryu et al., 2007). Smoke from biomass burning produces a large amount of fine particles (Pérez-Ramírez et al., 2017). The dense vegetation coverage in the Amazon region could also generate biogenic aerosols that are also fine particles (Carslaw et al., 2010).

Compared with Fig. 4b, aside from the greater coverage provided by the new product (Fig. 4a), Australia has the greatest differences in the magnitudes of FMF. FMF values in northern Australia from this study (0.5–0.6) are higher than MODIS FMF values there (0–0.3) and lower than in eastern Australia (FMF > 0.65). In India, MODIS FMFs are much lower than those from the new FMF product, especially in the east. The new global FMF product has a mean value of 0.6 in India, showing a maximum in the east (~0.8), but the MODIS FMF is almost 0–0.3 there. Jethva et al. (2010) found that the MODIS-derived FMF was significantly underestimated in India, and they also observed relatively low FMF values (close to zero) in many cases. East China shows significant differences between the two FMF products, where FMF values from this study are >0.65, and MODIS FMFs range from 0.3 to 0.5. The MODIS values and spatial distribution may be erroneous because aerosols in eastern China are predominantly affected by anthropogenic pollutants whose FMFs should thus be large, although dust aerosols may occasionally affect this region, especially in the spring (J. Liu et al., 2011). Industrialized urban areas and their surrounding regions in East Asia, including parts of China, Mongolia, Korea, Japan, and the northwestern Pacific, are characterized by predominantly anthropogenic pollutants, with an FMF of usually over 0.7 and an annually spatially averaged mean FMF of 0.68 ± 0.06 (Kim et al., 2007). FMF values from this study are greater than 0.8 in southern China. Mai et al. (2018) found that over the Pearl River Delta region, fine-mode particles comprised more than 90% of aerosol particles, in good agreement with our results.

Figures S3 and S4 further examine how the new global FMF and MODIS FMF products compare with AERONET FMF retrievals for the same collocated data volumes and how their respective accuracies are globally distributed, respectively. The new global FMF product performs better than the MODIS FMF product. Note that the agreements are generally better in heavily polluted regions like those in China and India where FMF values are high, presumably because of stronger signal-to-noise ratios.

Fig. 5 shows the spatial distributions of annual mean satellite-derived FMFs for the years 2008, 2011, 2014, and 2018. The distribution patterns in each year are similar to the multi-year distribution pattern, but regional differences between the years appear. For example, from 2008 to 2011, the FMF noticeably increased in northern North America, northern East Asia, and South Australia, but decreased in most areas of South America and Indonesia. From 2008 to 2014, the FMF increased in eastern India. This was also observed by Adak et al. (2014), who investigated atmospheric fine-mode particles over Darjeeling (a hill station in eastern India) and found that there was an increase in fine-mode aerosols in 2008, 2009, and 2010. Between 2011 and 2014, the FMF clearly increased more in northern North America, Europe, the Middle East, northern Asia, East Asia, and southern Africa. The most likely reason for this may be rapid worldwide economic development, accompanied by rising energy consumption and the intensification of human activities, resulting in a surge of anthropogenic aerosols, such as sulfate, ammonium nitrate, and organic and black carbon particles (Pozzer et al., 2015). Zhao et al. (2013) analyzed the variations in $PM_{2.5}$ concentration in Shenyang, China from 2010 to 2012 and found that the annual ratio of $PM_{2.5}/PM_{10}$ ranged from ~69.2% to 72.6%. They indicated that fine-mode aerosols were increasing mostly because of anthropogenic activity, in good agreement with our results. FMF concentrations generally decreased around the world from 2014 to 2017, with the greatest decrease occurring in China. There, the FMF decreased from ~0.8 to 0.6, likely due to the government emission control measures introduced in recent years (C. Li et al., 2017). For South America, where a decrease in FMF concentration occurred in the northern and eastern regions, there was an increase in the southwestern coastal areas.

3.2. Global land FMF trend analysis

Fig. 6a shows the linear trends of the new FMF product and the AERONET FMF data. In general, both show good agreement with the increasing and decreasing global trends, with 66.7% AERONET stations agreeing well. However, 33.3% of AERONET stations are not well-matched with the trend of the new FMF product. Opposite trends in the AERONET FMF and the new FMF data appear for some stations over the southern coast of the United States and southern Europe. In terms of magnitude, significant increasing trends (>+0.011 year^{-1}) appear in eastern and central Australia, north-central China, southern Sahara, India, Mexico, and the central United States. Significant decreasing trends (<-0.011 year^{-1}) are mainly observed in southern Asia and along the western coast of the United States. As linear regressions can be affected by outliers, autocorrelation, and heteroscedasticity of errors from input datasets (Hsu et al., 2012), the relative changes in the FMFs were also calculated using the new FMF product and AERONET FMF data to estimate the ten-year variations in global FMF. Fig. 6b shows the relative changes in FMF from both the new FMF product and the AERONET measurements; both sets show good agreement in the magnitude of change in most areas. Some underestimations of the relative changes in FMF appear over stations located in the southern coast of the United States, southern South America, and northern India, while overestimations occur over a few sporadic stations in the eastern coast of the United States, Central Asia, and eastern Europe. Large positive changes (>12%) are seen over the central United States, southern Sahara, northwestern China, and eastern and central Australia, while strong negative changes (<-12%) appear mainly in the western United States and southeastern Asia. The close result of the linear trends and relative changes indicate the reliability of the regions where large FMF

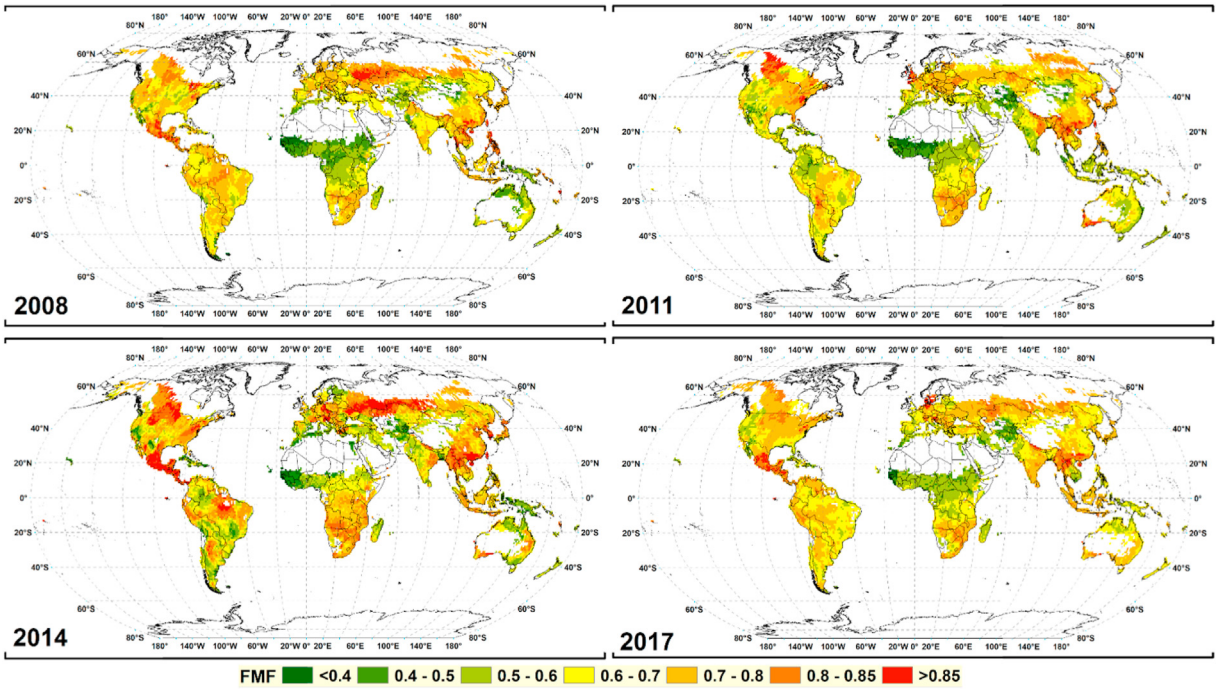

Fig. 5. Spatial distributions of the annual mean FMF between 2008 and 2017.

variations were detected. Regions in north-central China with an increasing FMF trend largely corresponded to regions in which the Three-North Shelter Forest Program was occurring. This program effectively increases local vegetation coverage and reduces desert areas (Yan et al., 2015), resulting in fewer local dust emissions. There are also positive FMF trends throughout, India, another country with a high population. India has suffered from acute $PM_{2.5}$ pollution in recent years as anthropogenic activities have significantly increased vehicular and industrial emissions (Babu et al., 2013; Mishra et al., 2019; Shaik et al., 2019). However, dust episodes in the Thar Desert have decreased from 2000 to 2009 (Kaskaoutis et al., 2011). In Australia, significant positive FMF trends are attributed mainly to an increase in biomass burning (i.e., bushfire) events (Haynes et al., 2010), a negative trend in dust emissions (Hammer et al., 2018). Weichenthal et al. (2017) indicated that biomass burning is an important source of ambient fine particulate matter that could lead to an increase in the ratio of fine-mode aerosols. The FMF has also increased significantly in the central United States, presumably due to the increase in agricultural practices and oil and gas operations from 2005 to 2015 (L. Zhang et al., 2017). In contrast, the FMF decreased over the western United States, and this might be associated with enhanced dust activity in the southwest (Tong et al., 2017).

3.3. Seasonal FMF characteristics and trends

The left column of Fig. 7 shows seasonal global land FMF spatial characteristics. Different seasons have different spatial distributions. In China, FMFs in the warm seasons of summer and autumn are generally higher than in the cool seasons of spring and winter. Long-range transport of springtime dust from the deserts in northern China increases the proportion of coarse particles, leading to lower FMFs in the northern part of East China (Huebert et al., 2003). In the warm seasons of East China, high relative humidity and temperature enhance the gas-to-particle conversion to create more secondary aerosols, increasing the amount of fine particles (Tan et al., 2015). Also, compared with the cool seasons, biogenic emissions are larger in summer when plant growth intensifies, generating a certain amount of submicron aerosols (Carslaw et al., 2010).

In India, the FMF in spring and summer (FMF < 0.6) is much lower than that in the autumn and winter (FMF > 0.7). Dust storms usually peak in the pre-monsoon period between March and May (Gautam et al., 2009), which is attributed to the low FMF values in this period. During the pre-monsoon months (spring), larger FMFs are observed over the east coast than over the west coast of India, indicating that coarse-mode aerosols dominate over the west coast of India. Kalapureddy and Devara (2008) also reported this phenomenon. Wintertime is when the highest FMF values in India occur. Ramachandran (2007) indicated that during winter, the boundary layer is low, and cold temperatures more likely trap pollutants, leading to hazy weather that gives rise to high FMF values. Moreover, during the post-monsoon seasons (autumn and winter), fine-mode aerosols due to bio-fuel, fossil fuel combustion, and biomass burning enhance the FMF in northern India. The shallow boundary layer and inactive convection further favor the accumulation of fine-mode aerosols (Sharma et al., 2017), inducing higher FMFs in autumn and winter than in spring and summer.

During all four seasons in the U.S., FMF values are highest in the eastern and central parts of the country. In the western U.S., FMFs in the warm seasons of summer and autumn are higher than in the cool seasons of spring and winter, similar to eastern China. In warm seasons, high temperature and humidity levels (Loría-Salazar et al., 2014) promote the formation of secondary aerosols and photochemical interactions, enhancing productions of sulfate (Tai et al., 2010) and secondary organic aerosols (Chu, 2004). The stagnant high-pressure systems present in warm seasons further favor the accumulation of fine-mode particles, resulting in higher FMFs in warm seasons (Tai et al., 2010). In cold seasons, concentrations of fine aerosols like sulfate are lower, and sea salt concentrations are at their highest (Hand et al., 2012), contributing to the lower FMF in coastal regions.

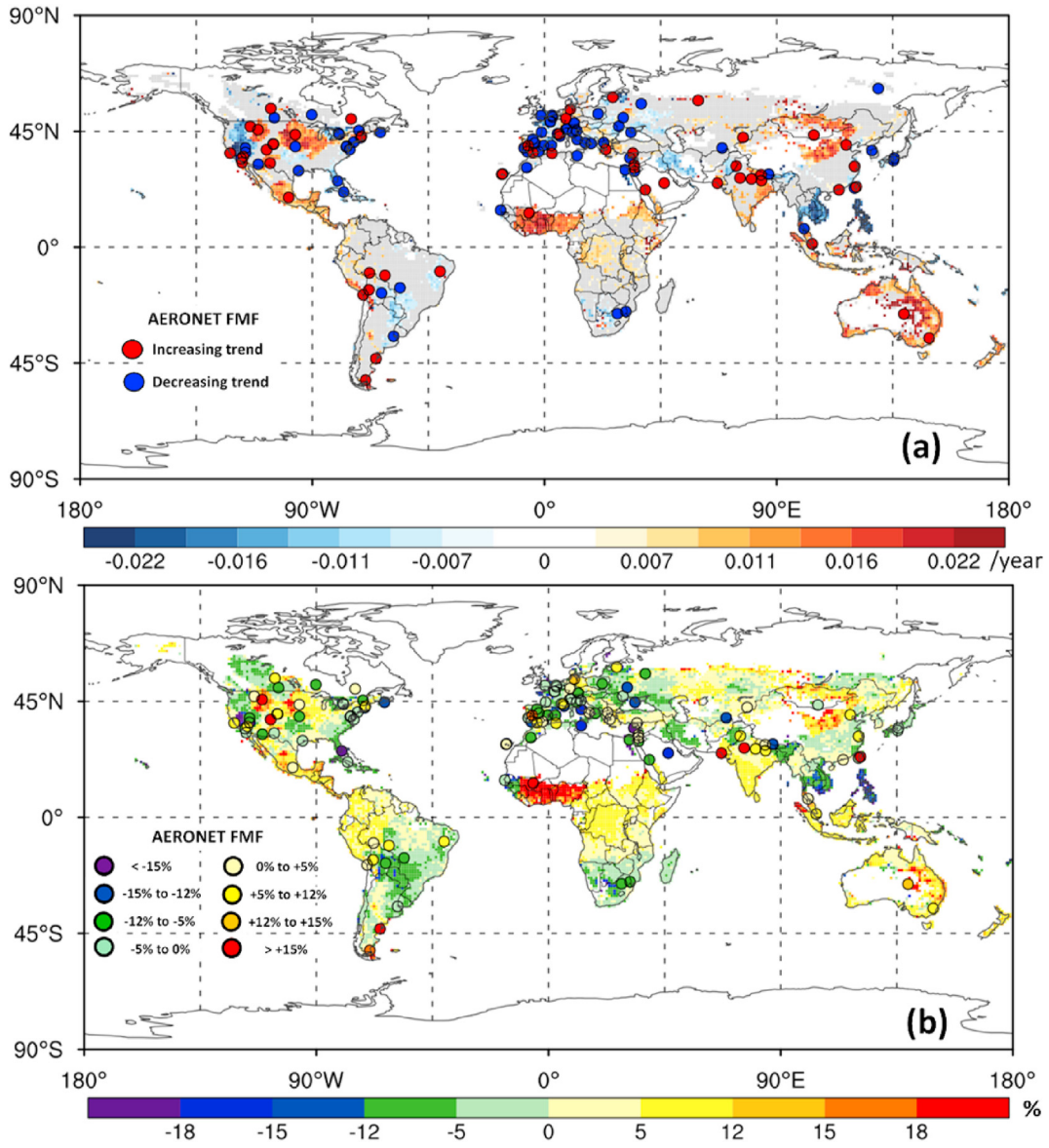

Fig. 6. (a) Ten-year (2008–2017) linear trends in the FMF from this study and AERONET measurements. In the base map, only pixels with a 95% significance of in linear trend analysis are shown with their trend values, while pixels with insignificant FMF trends are shown in gray. Furthermore, pixels with trends between ±0.005/year or fewer than 120 FMF retrievals/year are shown in white. The red and blue dots represent AERONET stations with significant increasing and decreasing trends, respectively, also at a 95% confidence level. (b) Ten-year (2008–2017) relative changes in the FMF calculated in this study (values shown in the color bar) and AERONET measurement (values shown as colored dots). Only stations with significant linear trends at a 95% confidence level are shown. (For interpretation of the references to color in this figure legend, the reader is referred to the Web version of this article.)

In Australia, the Amazon, and southern sub-tropical Africa, three hotspots of biomass burning, the FMF is higher in summer and autumn than in winter and spring. Located in the Southern Hemisphere, local biomass burning in these regions usually dominates the dry seasons starting in early summer and ending in the middle of autumn (Generoso et al., 2003; Perez-Ramirez et al., 2017). Biomass-burning smoke contributes greatly to fine-mode particles like black carbon and organic carbon, resulting in higher FMFs in dry seasons (Bond et al., 2013).

In Mediterranean Europe and northern Africa, the influx of coarse-mode particles from seasonal Saharan dust emissions impacts FMFs there. The FMF is lower in winter and spring than in summer and autumn, partly attributed to Saharan mineral dust particles that are transported towards Mediterranean Europe in spring (Floutsi et al., 2016; Gkikas et al., 2015) and dominating northern Africa in winter and spring (Klose et al., 2010). In general, the seasonal global land FMF distributions show that FMFs are higher in summer and autumn (warm seasons) and lower in spring and winter (cool seasons). These seasonal patterns also agree well with seasonal α' patterns, as shown in Figure S1. For example, a negative α' prevails over SA during the spring, while a positive α' appears in the summer, indicating that aerosols over SA are coarse-mode dominated in spring and fine-mode dominated in summer. This is also shown in the FMF data, with a higher FMF in summer (>0.6) than in spring (<0.5) over SA. Moreover, over NEA, a negative α' appears only in spring and a positive α' is shown in summer, autumn, and winter, reflecting that aerosols are coarse-mode dominated in spring. The FMF over NEA is also lower in spring

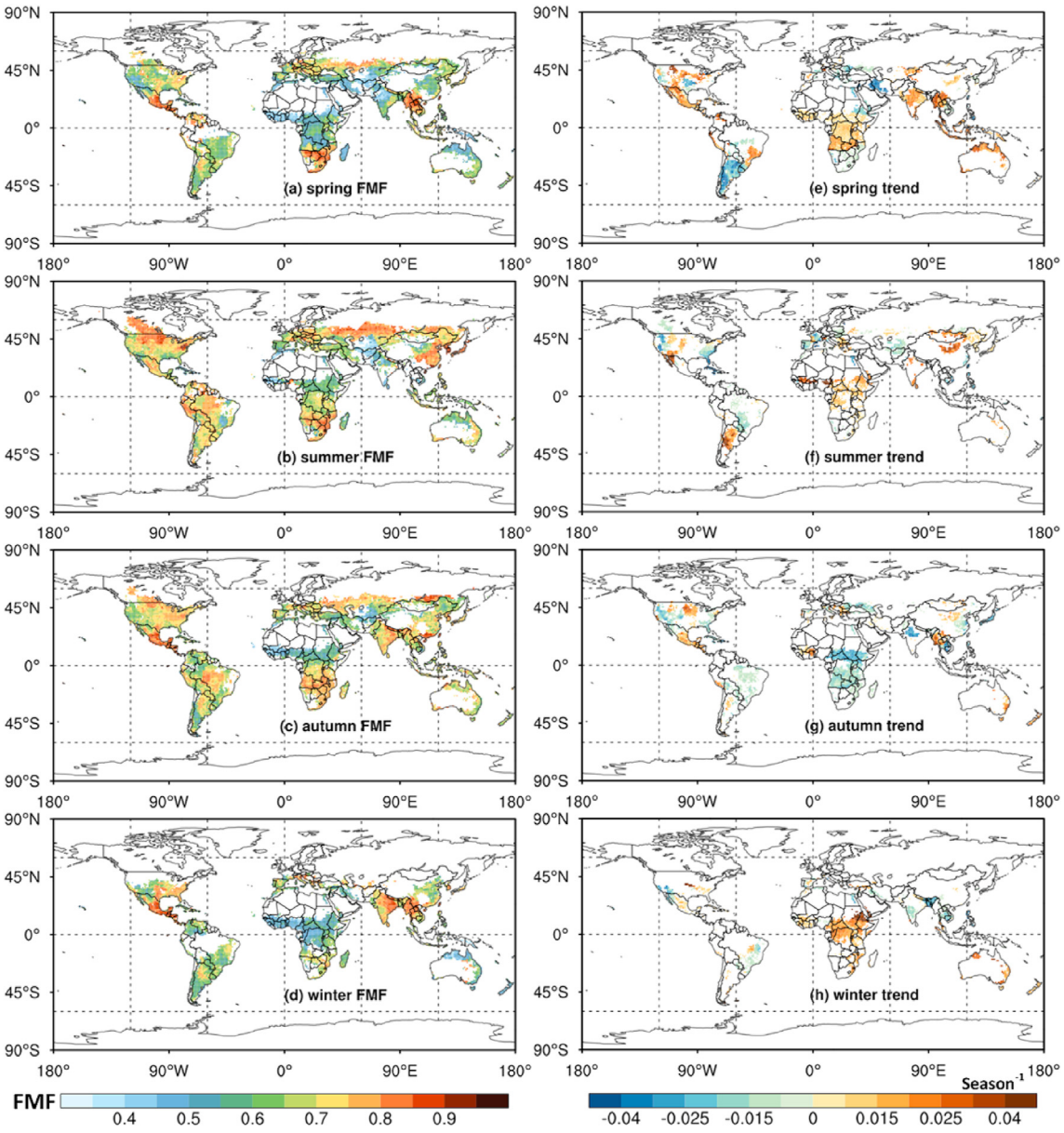

Fig. 7. Seasonal FMF distributions (left column) and trends (right column) from 2008 to 2017. The four seasons are defined as spring (March-April-May), summer (June-July-August), autumn (September-October-November), and winter (December-January-February). Only pixels for which there were 120 retrievals/year and 35 retrievals/season and for which the significance was over 95% from the linear trend are considered.

(<0.55) than in other seasons (>0.65), corresponding well with the α' patterns.

The right column of Fig. 7 shows seasonal FMF trends from 2008 to 2017. Seasonal FMF trends reflect long-term variations in such seasonal activities as biomass burning and dust storms that are further related to seasonal meteorological factors like monsoons, in particular, wind and rainfall. In India, the FMF trends show an increasing trend in spring and summer, significantly decreasing in autumn, then stabilizing in winter. The reduction in dust during the summer monsoon period (Jin and Wang, 2018) explains the increasing FMF trends in spring and summer. In the southern Sahara, the seasonal FMF trend is different between autumn (decreasing) and other seasons (increasing). Dust emissions vary little in the southern Sahara (Hammer et al., 2018), so the declining FMF trend may be due to the decrease in biomass burning in autumn when local biomass burning activities tend to peak during September and October (Ichoku et al., 2008). The FMF trends in the western U.S. are opposite to the trend in the central U.S. In the central U.S., the FMF increases, especially in autumn and spring. In northwestern China, significant FMF increases occur in spring and summer. The decreasing extent of dust source regions in spring in northwestern China (Hsu et al., 2012), would reduce emissions of coarse-mode aerosols, resulting in rising FMFs during this period. In Australia, all four seasons show increasing FMF trends especially strong in spring and winter. Considering that dust emission trends in Australia are insignificant (Shao et al., 2013), the increase in FMF may be due to the increasing amount of biomass-burning smoke during the past decade (Hsu et al., 2012). Clarke et al. (2013) indicated that increased fire weather conditions had been observed across Australia from 1973 to 2010, with the largest increases occurring in spring.

4. Concluding remarks

A new global satellite-based FMF product was developed from 2008 to 2017 based on MODIS data. The new FMF product was validated with AERONET FMF retrievals. The RMSE of the new FMF product used to analyze 169,313 valid data samples was 0.22. Comparisons made between the new global FMF product and the MODIS C5 FMF product show that the new product offers improvements in terms of retrieval coverage, regional features, and agreement with AERONET retrievals. The MODIS C5 FMF was significantly underestimated in most areas, with many unreasonably low values between 0 and 0.1. The spatial distributions of many MODIS FMF features appear unrealistic, consistent with results from other regional studies often based on in situ measurements.

Analyzed were the spatial distributions and temporal variations of the new FMF product. High FMF values (>0.8) were found in eastern North America, Mexico, central South Africa, Europe, northeastern Asia, southern Africa, and southern China. Low values (<0.5) occurred in the Sahelian and Sudanian zones of northern Africa. The trend in satellite-derived and AERONET FMFs in different countries is explored. The upward trend was particularly strong over Australia, implying that the proportion of fine particles increased since 2008. The global land FMF was higher in the warm seasons of summer and autumn and lower in the cool seasons of spring and winter. Note that some studies have also examined the spatiotemporal characteristics of the FMF (Ramachandran et al., 2007; Jethva et al., 2010). However, most of studies used ground-based measurements (Che et al., 2014; Zhao et al., 2013) or focused on a particular region (Tan et al., 2015). This study provides a new world view of FMF changes using a new satellite product. One finding opposite to that reported by others is that although the 10-year mean FMF was low in north-central China, there was a significant increasing trend in FMF in that region, suggesting that the Three-North Shelter Forest Program effectively reduced the fraction of large particles (2011–2020 is the fifth stage of this program). The Multi-angle Imaging Spectroradiometer AE product, however, showed an increase in the fraction of large particles in north-central China (Li, 2020). The promising results found in this study suggest that this newly developed FMF dataset can improve our understanding of global FMF changes. The new FMF dataset may be useful for studying the impact of fine-mode aerosols on Earth's environment and climate, e.g., estimating the global direct anthropogenic aerosol radiative forcing incurred by human activities. The global land FMF data developed in this study are available from the first author upon request (yanxing@bnu.edu.cn).

Credit author statement

Xing Yan: Conceptualization, Methodology, Software, Writing – original draft, Supervision. Zhou Zang: Investigation, Validation and Writing – original draft. Chen Liang: Validation. Nana Luo: Methodology, Writing – original draft. Rongmin Ren: Methodology. Maureen Cribb: Writing – review & editing. Zhanqing Li: Funding acquisition, Project administration, Writing – review & editing.

Declaration of competing interest

The authors declare that they have no known competing financial interests or personal relationships that could have appeared to influence the work reported in this paper.

Acknowledgments

This work was supported by the National Natural Science Foundation of China (42030606, 41801329 and 91837204), the National Key Research and Development Plan of China (2017YFC1501702), the Open Fund of State Key Laboratory of Remote Sensing Science (OFSLRSS201915) and the Fundamental Research Funds for the Central Universities. The authors gratefully acknowledge the MODIS and AERONET teams for their effort in making the data available.

Appendix A. Supplementary data

Supplementary data to this article can be found online at https://doi.org/10.1016/j.envpol.2021.116707.

References

Adak, A., Chatterjee, A., Singh, A.K., Sarkar, C., Ghosh, S., Raha, S., 2014. Atmospheric fine mode particulates at eastern Himalaya, India: role of meteorology, long-range transport and local anthropogenic sources. Aerosol and Air Quality Research 14 (1), 440–450.

Allen, R.J., Landuyt, W., Rumbold, S.T., 2016. An increase in aerosol burden and radiative effects in a warmer world. Nat. Clim. Change 6 (3), 269–274.

Babu, S.S., Manoj, M.R., Moorthy, K.K., et al., 2013. Trends in aerosol optical depth over Indian region: potential causes and impact indicators. J. Geophys. Res.: Atmosphere 118 (20), 11–794.

Bellouin, N., Boucher, O., Haywood, J., Reddy, M.S., 2005. Global estimate of aerosol direct radiative forcing from satellite measurements. Nature 438 (7071), 1138–1141.

Bond, T.C., Doherty, S.J., Fahey, D.W., et al., 2013. Bounding the role of black carbon in the climate system: a scientific assessment. J. Geophys. Res.: Atmosphere 118 (11), 5380–5552.

Carslaw, K.S., Boucher, O., Spracklen, D.V., Mann, G.W., Rae, J.G.L., Woodward, S., Kulmala, M., 2010. A review of natural aerosol interactions and feedbacks within the Earth system. Atmos. Chem. Phys. 10 (4).

Che, H., Gui, K., Xia, X., Wang, Y., Holben, B.N., Goloub, P., Cuevas-Agulló, E., Wang, H., Zheng, Y., Zhao, H., Zhang, X., 2019. Large contribution of meteorological factors to inter-decadal changes in regional aerosol optical depth. Atmos. Chem. Phys. 19, 10497–10523.

Che, H., Xia, X., Zhu, J., Li, Z., Dubovik, O., Holben, B., Goloub, P., Chen, H., Estelles, V., Cuevas-Agulló, E., Blarel, L., Wang, H., Zhao, H., Zhang, X., Wang, Y., Sun, J., Tao, R., Zhang, X., Shi, G., 2014. Column aerosol optical properties and aerosol radiative forcing during a serious haze-fog month over North China Plain in 2013 based on ground-based sunphotometer measurements. Atmos. Chem. Phys. 14, 2125–2138.

Che, H., Zhang, X., Chen, H., et al., 2009. Instrument calibration and aerosol optical depth validation of the China Aerosol Remote Sensing Network. J. Geophys. Res.: Atmosphere 114 (D3).

Chu, S.H., 2004. $PM_{2.5}$ episodes as observed in the speciation trends network. Atmos. Environ. 38 (31), 5237–5246.

Chung, C.E., Jung-Eun, C., Lee, Y., van Noije, T., Jeoung, H., Ha, K.J., Marks, M., 2016. Global fine-mode aerosol radiative effect, as constrained by comprehensive observations. Atmos. Chem. Phys. 16 (13), 8071.

Clarke, H., Lucas, C., Smith, P., 2013. Changes in Australian fire weather between 1973 and 2010. Int. J. Climatol. 33 (4), 931–944.

Dubovik, O., Smirnov, A., Holben, B.N., King, M.D., Kaufman, Y.J., Eck, T.F., Slutsker, I., 2000. Accuracy assessments of aerosol optical properties retrieved from AERONET Sun and sky-radiance measurements. J. Geophys. Res. 105, 9791–9806.

Dubovik, O., Holben, B., Eck, T.F., et al., 2002. Variability of absorption and optical properties of key aerosol types observed in worldwide locations. J. Atmos. Sci. 59 (3), 590–608.

Eck, T.F., Holben, B.N., Reid, J.S., et al., 1999. Wavelength dependence of the optical depth of biomass burning, urban, and desert dust aerosols. J. Geophys. Res.: Atmosphere 104 (D24), 31333–31349.

Eck, T.F., Holben, B.N., Sinyuk, A., et al., 2010. Climatological aspects of the optical properties of fine/coarse mode aerosol mixtures. J. Geophys. Res.: Atmosphere 115 (D19).

Floutsi, A.A., Korras-Carraca, M.B., Matsoukas, C., Hatzianastassiou, N., Biskos, G., 2016. Climatology and trends of aerosol optical depth over the Mediterranean basin during the last 12 years (2002–2014) based on Collection 006 MODIS-Aqua data. Sci. Total Environ. 551, 292–303.

Gassó, S., O'Neill, N., 2006. Comparisons of remote sensing retrievals and in situ measurements of aerosol fine mode fraction during ACE-Asia. Geophys. Res. Lett. 33 (5).

Gautam, R., Liu, Z., Singh, R.P., Hsu, N.C., 2009. Two contrasting dust-dominant periods over India observed from MODIS and CALIPSO data. Geophys. Res. Lett. 36 (6).

Generoso, S., Bréon, F.-M., Balkanski, Y., Boucher, O., Schulz, M., 2003. Improving the seasonal cycle and interannual variations of biomass burning aerosol sources. Atmos. Chem. Phys. 3, 1211–1222.

Gkikas, A., Houssos, E.E., Lolis, C.J., Bartzokas, A., Mihalopoulos, N., Hatzianastassiou, N., 2015. Atmospheric circulation evolution related to desert-dust episodes over the Mediterranean. Q. J. R. Meteorol. Soc. 141 (690),

1634–1645.
Hammer, M.S., Martin, R.V., Li, C., Torres, O., Manning, M., Boys, B.L., 2018. Insight into global trends in aerosol composition from 2005 to 2015 inferred from the OMI Ultraviolet Aerosol Index. Atmos. Chem. Phys. 18 (11).
Hand, J.L., Schichtel, B.A., Pitchford, M., Malm, W.C., Frank, N.H., 2012. Seasonal composition of remote and urban fine particulate matter in the United States. J. Geophys. Res.: Atmosphere 117 (D5).
Hatzianastassiou, N., Gkikas, A., Mihalopoulos, N., Torres, O., Katsoulis, B.D., 2009. Natural versus anthropogenic aerosols in the eastern Mediterranean basin derived from multiyear TOMS and MODIS satellite data. J. Geophys. Res.: Atmosphere 114 (D24).
Haynes, K., Handmer, J., McAneney, J., Tibbits, A., Coates, L., 2010. Australian bushfire fatalities 1900–2008: exploring trends in relation to the 'Prepare, stay and defend or leave early'policy. Environ. Sci. Pol. 13 (3), 185–194.
Holben, B.N., Eck, T.F., Slutsker, I.A., et al., 1998. AERONET—a federated instrument network and data archive for aerosol characterization. Rem. Sens. Environ. 66 (1), 1–16.
Hsu, N.C., Gautam, R., Sayer, A.M., Bettenhausen, C., Li, C., Jeong, M.J., Tsay, S.-C., Holben, B.N., 2012. Global and regional trends of aerosol optical depth over land and ocean using SeaWiFS measurements from 1997 to 2010. Atmos. Chem. Phys. 12, 8037–8053.
Huebert, B.J., Bates, T., Russell, P.B., et al., 2003. An overview of ACE-Asia: strategies for quantifying the relationships between Asian aerosols and their climatic impacts. J. Geophys. Res.: Atmosphere 108 (D23).
Ichoku, C., Giglio, L., Wooster, M.J., Remer, L.A., 2008. Global characterization of biomass-burning patterns using satellite measurements of fire radiative energy. Rem. Sens. Environ. 112 (6), 2950–2962.
IPCC, 2013. In: Stocker, T.F., Qin, D., Plattner, G.-K., Tignor, M., Allen, S.K., Boschung, J., Nauels, A., Xia, Y., Bex, V., Midgley, P.M. (Eds.), Climate Change 2013: the Physical Science Basis. Contribution of Working Group I to the Fifth Assessment Report of the Intergovernmental Panel on Climate Change. Cambridge University Press, Cambridge, United Kingdom and New York, NY, USA.
Jethva, H., Satheesh, S.K., Srinivasan, J., 2007. Assessment of second-generation MODIS aerosol retrieval (Collection 005) at Kanpur, India. Geophys. Res. Lett. 34 (19).
Jethva, H., Satheesh, S.K., Srinivasan, J., Levy, R.C., 2010. Improved retrieval of aerosol size-resolved properties from moderate resolution imaging spectroradiometer over India: role of aerosol model and surface reflectance. J. Geophys. Res.: Atmosphere 115 (D18).
Jin, Q., Wang, C., 2018. The greening of Northwest Indian subcontinent and reduction of dust abundance resulting from Indian summer monsoon revival. Sci. Rep. 8 (1), 1–9.
Kalapureddy, M.C.R., Devara, P.C.S., 2008. Characterization of aerosols over oceanic regions around India during pre-monsoon 2006. Atmos. Environ. 42 (28), 6816–6827.
Kaskaoutis, D.G., Kharol, S.K., Sinha, P.R., Singh, R.P., Badarinath, K.V.S., Mehdi, W., Sharma, M., 2011. Contrasting aerosol trends over South Asia during the last decade based on MODIS observations. Atmospheric Measurement Techniques Discussions 4 (4), 5275–5323.
Kaufman, Y.J., Tanré, D., Boucher, O., 2002. A satellite view of aerosols in the climate system. Nature 419 (6903), 215–223.
Kim, S.W., Yoon, S.C., Kim, J., Kim, S.Y., 2007. Seasonal and monthly variations of columnar aerosol optical properties over east Asia determined from multi-year MODIS, LIDAR, and AERONET Sun/sky radiometer measurements. Atmos. Environ. 41 (8), 1634–1651.
Kleidman, R.G., O'Neill, N.T., Remer, L.A., et al., 2005. Comparison of Moderate Resolution Imaging Spectroradiometer (MODIS) and Aerosol Robotic Network (AERONET) remote-sensing retrievals of aerosol fine mode fraction over ocean. J. Geophys. Res.: Atmosphere 110 (D22).
Klose, M., Shao, Y., Karremann, M.K., Fink, A.H., 2010. Sahel dust zone and synoptic background. Geophys. Res. Lett. 37 (9).
Komkoua Mbienda, A.J., Tchawoua, C., Vondou, D.A., Choumbou, P., Kenfack Sadem, C., Dey, S., 2017. Impact of anthropogenic aerosols on climate variability over Central Africa by using a regional climate model. Int. J. Climatol. 37 (1), 249–267.
Kumar, K.R., Sivakumar, V., Yin, Y., et al., 2014. Long-term (2003–2013) climatological trends and variations in aerosol optical parameters retrieved from MODIS over three stations in South Africa. Atmos. Environ. 95, 400–408.
Levy, R.C., Mattoo, S., Munchak, L.A., Remer, L.A., Sayer, A.M., Patadia, F., Hsu, N.C., 2013. The Collection 6 MODIS aerosol products over land and ocean. Atmospheric Measurement Techniques 6 (11), 2989.
Levy, R.C., Mattoo, S., Sawyer, V., Shi, Y., Colarco, P.R., Lyapustin, A.I., et al., 2018. Exploring systematic offsets between aerosol products from the two MODIS sensors. Atmospheric Measurement Techniques 11 (7), 4073–4092.
Levy, R.C., Remer, L.A., Mattoo, S., Vermote, E.F., Kaufman, Y.J., 2007. Second-generation operational algorithm: retrieval of aerosol properties over land from inversion of Moderate Resolution Imaging Spectroradiometer spectral reflectance. J. Geophys. Res.: Atmosphere 112 (D13).
Li, C., McLinden, C., Fioletov, V., et al., 2017. India is overtaking China as the world's largest emitter of anthropogenic sulfur dioxide. Sci. Rep. 7 (1), 1–7.
Li, J., 2020. Pollution trends in China from 2000 to 2017: a multi-sensor view from space. Rem. Sens. 12 (2), 208.
Li, J., Han, X., Jin, M., Zhang, X., Wang, S., 2019. Globally analysing spatiotemporal trends of anthropogenic PM2. 5 concentration and population's PM2. 5 exposure from 1998 to 2016. Environ. Int. 128, 46–62.
Li, Z.Q., Xu, H., Li, K.T., et al., 2018. Comprehensive study of optical, physical, chemical, and radiative properties of total columnar atmospheric aerosols over China: an overview of Sun–Sky Radiometer Observation Network (SONET) measurements. Bull. Am. Meteorol. Soc. 99 (4), 739–755.
Liu, J., Zheng, Y., Li, Z., Flynn, C., Welton, E.J., Cribb, M., 2011. Transport, vertical structure and radiative properties of dust events in southeast China determined from ground and space sensors. Atmos. Environ. 45 (35), 6469–6480.
Liu, Y., Cai, W., Sun, C., et al., 2019. Anthropogenic aerosols cause recent pronounced weakening of Asian Summer Monsoon relative to last four centuries. Geophys. Res. Lett. 46 (10), 5469–5479.
Loría-Salazar, S.M., Arnott, W.P., Moosmueller, H., 2014. Accuracy of near-surface aerosol extinction determined from columnar aerosol optical depth measurements in Reno, NV, USA. J. Geophys. Res.: Atmosphere 119 (19), 11–355.
Luo, N., An, L., Nara, A., Yan, X., Zhao, W., 2016. GIS-based multielement source analysis of dustfall in Beijing: a study of 40 major and trace elements. Chemosphere 152, 123–131.
Luo, N., Wong, M.S., Zhao, W., Yan, X., Xiao, F., 2015. Improved aerosol retrieval algorithm using Landsat images and its application for PM10 monitoring over urban areas. Atmos. Res. 153, 264–275.
Lyapustin, A., Wang, Y., Korkin, S., Huang, D., 2018. MODIS Collection 6 MAIAC algorithm. Atmospheric Measurement Techniques 11 (10), 5741–5765.
Mai, B., Deng, X., Xia, X., et al., 2018. Column-integrated aerosol optical properties of coarse-and fine-mode particles over the Pearl River Delta region in China. Sci. Total Environ. 622, 481–492.
Mehta, M., Singh, R., Singh, A., Singh, M., Anshumali, 2016. Recent global aerosol optical depth variations and trends — a comparative study using MODIS and MISR level 3 datasets. Rem. Sens. Environ. 181, 137–150.
Mishra, R.K., Pandey, A., Pandey, G., Kumar, A., 2019. The effect of odd-even driving scheme on PM2. 5 and PM1. 0 emission. Transport. Res. Transport Environ. 67, 541–552.
Nakata, M., Sano, I., Mukai, S., 2017. July). Response of the climate system to anthropogenic aerosols. In: 2017 IEEE International Geoscience and Remote Sensing Symposium (IGARSS). IEEE, pp. 5946–5949.
O'Neill, N.T., Dubovik, O., Eck, T.F., 2001. Modified Ångström exponent for the characterization of submicrometer aerosols. Appl. Optic. 40 (15), 2368–2375.
O'Neill, N.T., Eck, T.F., Smirnov, A., Holben, B.N., Thulasiraman, S., 2003. Spectral discrimination of coarse and fine mode optical depth. J. Geophys. Res.: Atmosphere 108 (D17).
Pérez-Ramírez, D., Andrade-Flores, M., Eck, T.F., et al., 2017. Multi year aerosol characterization in the tropical Andes and in adjacent Amazonia using AERONET measurements. Atmos. Environ. 166, 412–432.
Pozzer, A., De Meij, A., Yoon, J., Tost, H., Georgoulias, A.K., Astitha, M., 2015. AOD trends during 2001–2010 from observations and model simulations. Atmos. Chem. Phys. 15 (10), 5521–5535.
Ramachandran, S., 2007. Aerosol optical depth and fine mode fraction variations deduced from Moderate Resolution Imaging Spectroradiometer (MODIS) over four urban areas in India. J. Geophys. Res.: Atmosphere 112 (D16).
Redemann, J., Zhang, Q., Livingston, J., et al., 2009. Testing aerosol properties in MODIS Collection 4 and 5 using airborne sunphotometer observations in INTEX-B/MILAGRO. Atmos. Chem. Phys. 9 (21).
Remer, L.A., Kaufman, Y.J., Tanré, D., et al., 2005. The MODIS aerosol algorithm, products, and validation. J. Atmos. Sci. 62 (4), 947–973.
Ruiz-Arias, J.A., Dudhia, J., Gueymard, C.A., Pozo-Vázquez, D., 2013. Assessment of the Level-3 MODIS daily aerosol optical depth in the context of surface solar radiation and numerical weather modeling. Atmos. Chem. Phys. 13 (2), 675–692.
Ryu, S.Y., Kwon, B.G., Kim, Y.J., Kim, H.H., Chun, K.J., 2007. Characteristics of biomass burning aerosol and its impact on regional air quality in the summer of 2003 at Gwangju, Korea. Atmos. Res. 84 (4), 362–373.
Sayer, A.M., Hsu, N.C., Bettenhausen, C., Jeong, M.J., Meister, G., 2015. Effect of MODIS Terra radiometric calibration improvements on collection 6 deep blue aerosol products: validation and terra/aqua consistency. J. Geophys. Res.: Atmosphere 120 (23), 12–157.
Sayer, A.M., Munchak, L.A., Hsu, N.C., Levy, R.C., Bettenhausen, C., Jeong, M.J., 2014. MODIS Collection 6 aerosol products: comparison between Aqua's e-Deep Blue, Dark Target, and "merged" data sets, and usage recommendations. J. Geophys. Res.: Atmosphere 119 (24), 13–965.
Shaik, D.S., Kant, Y., Mitra, D., et al., 2019. Impact of biomass burning on regional aerosol optical properties: a case study over northern India. J. Environ. Manag. 244, 328–343.
Shao, Y., Klose, M., Wyrwoll, K.H., 2013. Recent global dust trend and connections to climate forcing. J. Geophys. Res.: Atmosphere 118 (19), 11–107.
Sharma, S.K., Mandal, T.K., Saxena, M., 2017. Inter-annual variation of ambient ammonia and related trace gases in Delhi, India. Bull. Environ. Contam. Toxicol. 99 (2), 281–285.
Singh, D., Bollasina, M., Ting, M., Diffenbaugh, N.S., 2019. Disentangling the influence of local and remote anthropogenic aerosols on South Asian monsoon daily rainfall characteristics. Clim. Dynam. 52 (9–10), 6301–6320.
Smirnov, A., Holben, B.N., Eck, T.F., Dubovik, O., Slutsker, I., 2000. Cloud-screening and quality control algorithms for the AERONET database. Remote Sens. Environ. 73 (3), 337–349.
Tai, A.P., Mickley, L.J., Jacob, D.J., 2010. Correlations between fine particulate matter (PM2. 5) and meteorological variables in the United States: implications for the sensitivity of PM2. 5 to climate change. Atmos. Environ. 44 (32), 3976–3984.
Takamura, T., 2004. Overview of SKYNET and its activities. Opt. Pura Apl. 37 (3),

3303–3308.
Tan, C., Zhao, T., Xu, X., Liu, J., Zhang, L., Tang, L., 2015. Climatic analysis of satellite aerosol data on variations of submicron aerosols over East China. Atmos. Environ. 123, 392–398.
Tong, D.Q., Wang, J.X., Gill, T.E., Lei, H., Wang, B., 2017. Intensified dust storm activity and Valley fever infection in the southwestern United States. Geophys. Res. Lett. 44 (9), 4304–4312.
Turco, M., Rosa-Cánovas, J.J., Bedia, J., Jerez, S., Montávez, J.P., Llasat, M.C., Provenzale, A., 2018. Exacerbated fires in Mediterranean Europe due to anthropogenic warming projected with non-stationary climate-fire models. Nat. Commun. 9 (1), 1–9.
Tutsak, E., Koçak, M., 2019. Long-term measurements of aerosol optical and physical properties over the Eastern Mediterranean: hygroscopic nature and source regions. Atmos. Environ. 207, 1–15.
Weichenthal, S., Kulka, R., Lavigne, E., et al., 2017. Biomass burning as a source of ambient fine particulate air pollution and acute myocardial infarction. Epidemiology 28 (3), 329.
Yan, Q., Zhu, J., Zheng, X., Jin, C., 2015. Causal effects of shelter forests and water factors on desertification control during 2000–2010 at the Horqin Sandy Land region, China. J. For. Res. 26 (1), 33–45.
Yan, X., Li, Z., Luo, N., et al., 2019. An improved algorithm for retrieving the fine-mode fraction of aerosol optical thickness. Part 2: application and validation in Asia. Remote Sens. Environ. 222, 90–103.
Yan, X., Li, Z., Luo, N., Shi, W., Zhao, W., Yang, X., Jin, J., 2018. A minimum albedo aerosol retrieval method for the new-generation geostationary meteorological satellite Himawari-8. Atmos. Res. 207, 14–27.
Yan, X., Li, Z., Shi, W., Luo, N., Wu, T., Zhao, W., 2017b. An improved algorithm for retrieving the fine-mode fraction of aerosol optical thickness, part 1: algorithm development. Remote Sens. Environ. 192, 87–97.
Yan, X., Shi, W., Li, Z., et al., 2017a. Satellite-based $PM_{2.5}$ estimation using fine-mode aerosol optical thickness over China. Atmos. Environ. 170, 290–302.
Yan, X., Zang, Z., Luo, N., Jiang, Y., Li, Z., 2020. New interpretable deep learning model to monitor real-time PM2.5 concentrations from satellite data. Environ. Int. 144.
Yang, X., Jiang, L., Zhao, W., Xiong, Q., Zhao, W., Yan, X., 2018. Comparison of ground-based PM2. 5 and PM10 concentrations in China, India, and the US. Int. J. Environ. Res. Publ. Health 15 (7), 1382.
Yang, X., Zhao, C., Luo, N., Zhao, W., Shi, W., Yan, X., 2020. Evaluation and Comparison of Himawari-8 L2 V1. 0, V2. 1 and MODIS C6. 1 aerosol products over Asia and the oceania regions. Atmos. Environ. 220, 117068.
Zhang, L., Henze, D.K., Grell, G.A., Torres, O., Jethva, H., Lamsal, L.N., 2017. What factors control the trend of increasing AAOD over the United States in the last decade? J. Geophys. Res.: Atmosphere 122 (3), 1797–1810.
Zhang, Y., Li, Z., 2015. Remote sensing of atmospheric fine particulate matter ($PM_{2.5}$) mass concentration near the ground from satellite observation. Rem. Sens. Environ. 160, 252–262.
Zhao, H., Che, H., Zhang, X., Ma, Y., Wang, Y., Wang, H., Wang, Y., 2013. Characteristics of visibility and particulate matter (PM) in an urban area of Northeast China. Atmospheric Pollution Research 4 (4), 427–434.
Zheng, X., Zhao, W., Yan, X., Shu, T., Xiong, Q., Chen, F., 2015. Pollution characteristics and health risk assessment of airborne heavy metals collected from Beijing bus stations. Int. J. Environ. Res. Publ. Health 12, 9658–9671.